COVER SHEET

Paper Number: **1802**

Title: **Fracture of Carbon Nanotube - Amorphous Carbon Composites: Molecular Modeling**

Authors: Benjamin D. Jensen[1,2]
Kristopher E. Wise[1]
Gregory M. Odegard[2]

ABSTRACT

Carbon nanotubes (CNTs) are promising candidates for use as reinforcements in next generation structural composite materials because of their extremely high specific stiffness and strength. They cannot, however, be viewed as simple replacements for carbon fibers because there are key differences between these materials in areas such as handling, processing, and matrix design. It is impossible to know for certain that CNT composites will represent a significant advance over carbon fiber composites before these various factors have been optimized, which is an extremely costly and time intensive process.

This work attempts to place an upper bound on CNT composite mechanical properties by performing molecular dynamics simulations on idealized model systems with a reactive forcefield that permits modeling of both elastic deformations and fracture. Amorphous carbon (AC) was chosen for the matrix material in this work because of its structural simplicity and physical compatibility with the CNT fillers. It is also much stiffer and stronger than typical engineering polymer matrices. Three different arrangements of CNTs in the simulation cell have been investigated: a single-wall nanotube (SWNT) array, a multi-wall nanotube (MWNT) array, and a SWNT bundle system. The SWNT and MWNT array systems are clearly idealizations, but the SWNT bundle system is a step closer to real systems in which individual tubes aggregate into large assemblies. The effect of chemical crosslinking on composite properties is modeled by adding bonds between the CNTs and AC. The balance between weakening the CNTs and improving fiber-matrix load transfer is explored by systematically varying the extent of crosslinking.

It is, of course, impossible to capture the full range of deformation and fracture processes that occur in real materials with even the largest atomistic molecular dynamics simulations. With this limitation in mind, the simulation results reported here provide a plausible upper limit on achievable CNT composite properties and yield some insight on the influence of processing conditions on the mechanical properties of CNT composites.

1, Advanced Materials and Processing Branch, NASA Langley Research Center, Mail Stop 226, Hampton, VA, 23681-2199, U.S.A.

2, Department of Mechanical Engineering - Engineering Mechanics, Michigan Technological University, 1400 Townsend Dr., Houghton, MI, 49931, U.S.A.

INTRODUCTION

Because of their extremely high stiffness and strength, carbon nanotubes (CNTs) are promising candidates for use as reinforcement in composite materials. Realizing this potential in production materials will require optimization of intertube load transfer because individual CNTs are substantially shorter than any component-scale composite that might be made with them. The results presented in this work are a first step towards achieving a systematic understanding of how the structure and bonding in CNT-based composites affect their bulk mechanical properties.

Load transfer between CNTs, whether directly between tubes or through the matrix, occurs either through covalent bonds or van der Waals interactions. Covalent bonds result in much larger intertube load transfer, but their formation effectively creates defects in the tube structure, reducing intratube mechanical properties. Conversely, van der Waals interactions yield relatively weak intertube load transfer, but do not weaken the CNTs by disrupting their structure. Although each individual van der Waals interaction is relatively weak, their vast numbers have a significant effect on CNT mesoscale structure, as manifested in the strong tendency of CNTs to agglomerate into large bundles of hundreds or thousands of tubes. While this aggregation occurs spontaneously and is, in fact, very difficult to prevent or reverse, covalent crosslinking must be created by chemical functionalization or irradiation [1-2]. The effects of tube bundling and the extent of covalent crosslinking on nanocomposite mechanical properties are two of the key issues addressed in this study.

While the fiber reinforcement dominates the bulk mechanical properties of composites, the matrix material can also make a significant contribution. Because exploring the upper limits of plausibly achievable CNT composite properties is also a goal of this work, amorphous carbon (AC) was selected for the matrix. AC has a much higher stiffness and strength than structural polymers [3-4] and also exhibits good structural and chemical compatibility with the CNTs.

CNT/AC composites were investigated using molecular dynamics (MD) simulations with the reactive force field ReaxFF. The simulations were aimed at assessing the effect of crosslinking, CNT bundling, and the type of CNT, single-walled nanotube (SWNT) or multi-walled nanotube (MWNT), on the mechanical behavior of CNT/AC composites. To achieve this, three different CNT/AC composite system types were modeled: SWNTs in a uniformly spaced array, MWNTs in a uniformly spaced array, and SWNTs arranged in bundles. For each of the three composite system types, five models were created with an increasing extent of covalent crosslinking between the CNTs and AC. Although the bonding changed slightly during the simulations, the nominal percentages of CNT atoms crosslinked to the matrix were 0%, 5%, 10%, 15%, and 20%. For each system, the full elastic stiffness tensor was calculated and used to derive engineering constants such as Young's modulus, shear modulus, and Poisson's ratio. In addition, the tensile fracture properties in the axial and transverse directions were investigated, allowing the calculation of ultimate strength. The composite properties are compared with previously reported results for the pure component systems [4].

COMPUTATIONAL DETAILS

The ReaxFF reactive forcefield, as implemented in the open source MD program LAMMPS, was used for all simulations described in this work [5-6]. All of the potential energy terms involving covalent interactions in ReaxFF depend on the bond order function, a continuous function of the interatomic distance that goes to zero beyond covalent bond distances. The potential energy is composed of many independent contributions, including bonds, angles, dihedrals, van der Waals, electrostatic, over/under coordination, conjugation, hydrogen bonding, and other small terms [7]. The $ReaxFF_{C\text{-}2013}$ carbon parameterization of Srinivasan *et al*. [8], which has been shown to accurately describe the elastic and fracture properties of AC and CNTs [4], was used for this work.

The three different composite material systems simulated in this work are shown in Figure 1. The first system is an evenly spaced hexagonal array of fourteen SWNTs (Figure 1a). The second system is an evenly spaced hexagonal array of four MWNTs (Figure 1b). The third system is composed of fourteen SWNTs arranged into two bundles (Figure 1c). The first two systems are idealized model systems in which the nanotubes are perfectly dispersed. The third system is more representative of the structures observed in experimental materials in which the CNTs tend to aggregate into bundles that are difficult to separate or penetrate with the matrix [9]. This third system allows for the effect of bundling to be compared to the ideally dispersed systems. The SWNTs in the array and bundled system are identical except for their arrangement. The SWNTs have a chiral index of (20,0), which corresponds to a diameter of 1.5 nm. The MWNTs are composed of three walls with chiralities of (32,0), (23,0), and (14,0), yielding an outer wall diameter of 2.5 nm and wall spacing of 0.34 nm. All of the CNTs had lengths of 10.2 nm and were continuous across the periodic boundary. All of the structural images in this paper were rendered using the open source Ovito program [10].

The simulation cells were designed to maintain an AC:CNT mass ratio of 167:100 for all systems. Both SWNT systems contained 71,890 atoms and the MWNT systems contained 70,863 atoms. The size of the simulation box and the spacing between CNTs or CNT bundles was set to meet two requirements: the 167:100 AC:CNT mass ratio and an initial AC density of 3.0 g/cm^3. This resulted in SWNT arrays with transverse box lengths of 17.6 nm and 4.4 nm, MWNT arrays with box lengths of 8.3 nm and 7.2 nm, and SWNT bundles with box lengths of 6.7 nm and 11.6 nm. After equilibration, the density of the AC matrix for each material system was found to be about 2.4 g/cm^3. This falls

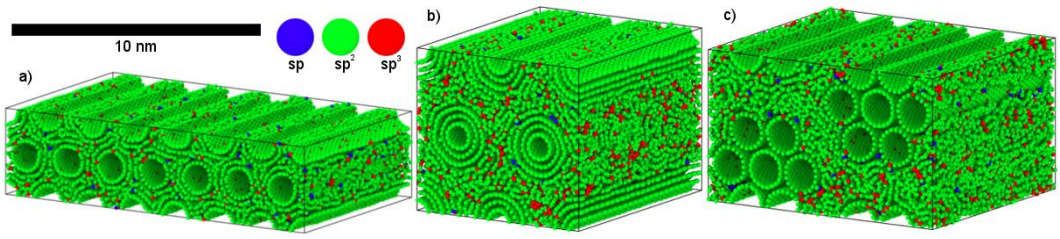

Figure 1. Equilibrated (a) SWNT array crosslinked at 4% (b) MWNT array crosslinked at 4% (c) SWNT bundles crosslinked at 5%.

within the range of reported experimental AC densities, which varies from 0.9 – 3.3 g/cm^3 [11], depending on processing conditions.

For each of the three system types, five independent models were created with nominal crosslinking fractions of 0%, 5%, 10%, 15% and 20%. The crosslinking fraction is determined by dividing the number of CNT atoms directly bonded to the matrix by the total number of CNT atoms directly exposed to the matrix. So for the case of the MWNT array system, only the atoms in the exterior nanotube wall are counted because the inner tubes are not exposed to the matrix. In the case of the SWNT bundle system, only the matrix-facing 2/3 of the outer six nanotubes are counted because the inward facing atoms of the outer tubes and the atoms of the central tube cannot form crosslinks to the matrix. All of the atoms in the SWNT array are counted because any of them could form a crosslink. Direct CNT-CNT crosslinking was not considered in this work.

At the beginning of the equilibration procedure, initial crosslink sites were selected at random from a list of candidate CNT atoms and an AC atom was placed within bonding distance. New crosslinks were allowed to form and pre-seeded crosslinking sites were free to break during the equilibration procedure. The pre-equilibration systems were created with crosslink fractions of 0%, 5%, 10%, 25%, and 50%. While the amount of crosslinking changed very little during the course of equilibration for the 0%, 5%, and 10% systems, substantial reductions occurred in the 25% and 50% systems. The final crosslinking fractions were found to be about 15% and 20%, respectively, for the latter two systems. For each combination of material system and degree of crosslinking, two simulation cells were independently constructed and equilibrated. Running the complete set of simulations on two independent simulation systems allows for the identification of spurious results and for an assessment of the statistical scatter between repeated runs. Using two replicas of each of the three material systems at five different degrees of crosslinking resulted in a total of 30 simulation runs.

A summary of the equilibration procedure is given in Table I. In steps A-D the CNT and AC atoms are placed in their initial positions and any pairs of atoms in close contact are separated. In anticipation of the system expanding at the end of the equilibration procedure, the CNTs were axially compressed by 4%-5% before the AC atoms were placed. In steps E-K the system was heated to 1,200 K, held at that temperature for 150 ps, and then cooled to 300 K at a rate of 10 K/ps. At the end of step K, there was a significant residual stress in the material resulting from the mismatch of the optimal equilibrium box length for the AC and CNTs. Steps L-Q were used to reduce this residual stress. At the end of the equilibration procedure, the residual stress in the AC component was on the order of 3 GPa. This is consistent with experimental results showing that AC films can have bulk residual stresses on the order of 5 GPa [12]. These residual stresses, while seemingly large, correspond to relatively small strains in the system, typically less than 2%, due to the high stiffness of both the AC and CNT constituents. Therefore, the residual stresses in these systems are considered to be within an acceptable range for determining mechanical properties. The equilibrated systems have an average CNT volume fraction of 52±1% for the SWNT systems and 42±1% for the MWNT systems. The simulation cell densities are 1.83±0.03 g/cm^3 for the SWNT systems and 2.32±0.03 g/cm^3 for the MWNT systems.

TABLE I. EQUILIBRATION PROCEDURE

Step	Time	Description
A	-	Place CNT atoms Place AC atoms at pre-selected crosslink sites
B	20 ps	Minimize coordinates and box in the axial direction
C	-	Compress system 4%-5% in the axial direction Immobilize CNT and crosslink atoms Place remaining AC atoms
D	12 ps	Run low-temperature damped dynamics
E	60 ps	Heat to 1,200 K at 20 K/ps
F	150 ps	Maintain 1,200 K
G	90 ps	Cool to 300 K at 10 K/ps
H	25 ps	Relax transverse box dimensions
I	-	Unfreeze CNT and crosslink atoms
J	25 ps	Relax all box directions (NPT)
K	5 ps	Maintain system temperature at fixed volume (NVT)
L	-	Strain axial box direction 0-5%
M	5 ps	Heat to 1,200 K
N	5 ps	Maintain 1,200 K
O	45 ps	Cool at 20 K/ps
P	50 ps	Relax all box directions (NPT)
Q	5 ps	Maintain system in NVT
R	-	Repeat steps L-Q

Elastic properties were predicted using the equivalent continuum method [13] in which stresses and strains are related by the stiffness tensor shown in Equation 1. The CNT/AC composites are transversely isotropic, and the CNT axes are aligned in the 1 direction.

$$\begin{bmatrix}\sigma_{11}\\ \sigma_{22}\\ \sigma_{33}\\ \sigma_{23}\\ \sigma_{13}\\ \sigma_{12}\end{bmatrix} = \begin{bmatrix} C_{11} & C_{12} & C_{12} & 0 & 0 & 0 \\ & C_{22} & C_{23} & 0 & 0 & 0 \\ & & C_{22} & 0 & 0 & 0 \\ & & & C_{44} & 0 & 0 \\ & symm. & & & C_{66} & 0 \\ & & & & & C_{66} \end{bmatrix} \begin{bmatrix}\varepsilon_{11}\\ \varepsilon_{22}\\ \varepsilon_{33}\\ 2\varepsilon_{23}\\ 2\varepsilon_{13}\\ 2\varepsilon_{12}\end{bmatrix} \quad (1)$$

The σ_{ij} are components of the stress tensor, C_{ij} are components of the stiffness tensor, and ε_{ij} are components of the strain tensor. The stiffness tensor and engineering constants (Young's modulus, Poisson's ratio, and shear modulus) are inversely related as shown in Equation 2, where E_i is the Young's modulus in the i direction, v_{ij} is the Poisson's ratio associated with the i and j directions, and $G_{ij}$is the shear modulus in the ij plane.

$$\begin{bmatrix} C_{11} & C_{12} & C_{12} & 0 & 0 & 0 \\ & C_{22} & C_{23} & 0 & 0 & 0 \\ & & C_{22} & 0 & 0 & 0 \\ & & & C_{44} & 0 & 0 \\ & symm. & & & C_{66} & 0 \\ & & & & & C_{66} \end{bmatrix}^{-1} = \begin{bmatrix} \frac{1}{E_1} & \frac{-\nu_{12}}{E_1} & \frac{-\nu_{12}}{E_1} & 0 & 0 & 0 \\ & \frac{1}{E_2} & \frac{-\nu_{23}}{E_2} & 0 & 0 & 0 \\ & & \frac{1}{E_2} & 0 & 0 & 0 \\ & & & \frac{1}{G_{23}} & 0 & 0 \\ & symm. & & & \frac{1}{G_{12}} & 0 \\ & & & & & \frac{1}{G_{12}} \end{bmatrix} \quad (2)$$

The stiffness coefficients for each material were determined through a set of six simulations. For each simulation, the box and atomic coordinates were scaled in one of the six strain directions, three axial and three shear, while the remaining five strain components were set to zero. Each simulation therefore produced one column of the stiffness tensor. Each system was strained to 0.25%, 0.50% and 1.00%, and each was found to exhibit a linear response over this range. Strained systems were relaxed for 10 ps at constant volume at 300 K using a Berendsen thermostat. The potential energy and stress in the systems plateaued well within the 10 ps relaxation time. The pressure difference was calculated between the last 5 ps of the strained and unstrained system simulations. Stiffness tensor coefficients were computed using Equation 1 and the computed pressure difference and strains. The results from the three strains and the symmetric components of the stiffness tensor were averaged together.

The ultimate tensile strength and fracture properties were determined by straining each system in uniaxial tension. During the tensile simulations, contractions transverse to the tensile axis were allowed by maintaining the pressures at zero in the transverse directions using a Berendsen barostat. The models were deformed at a true strain rate of 1.5 ns^{-1}. This strain rate was selected based on previous studies of AC and CNTs using $ReaxFF_{C\text{-}2013}$ [4]. The ultimate tensile strength was determined by locating the maximum stress value in the stress-strain response and averaging over the previous 2 ps to reduce the effects of instantaneous thermal fluctuations

Mechanical properties in this work are reported in specific units of GPa/(g/cm^3). CNT mechanical properties are typically reported by approximating the CNT volume to be that of an equivalent hollow cylinder with a wall thickness equal to the van der Waals diameter of carbon, 0.34 nm. Use of this thin-shell approximation of the volume provides consistency when comparing predicted properties of various diameters of CNTs to each other or to graphene. For composite materials, however, it is more appropriate to assign all sub-volumes within a repeat unit cell to specific material phases such that the total volume fractions of each of the phases sums to unity. As a result, this approach implicitly assumes that CNTs have the volumes of solid cylinders, as opposed to hollow cylinders. The co-existence of these two different approaches in the literature leads to a large discrepancy in the reported mechanical properties of individual CNT molecules and bulk CNT materials. This issue is mitigated in this work by using specific units, which are independent of the volumes of the system or sub-systems, depending only on the number and strength of the atomic bonds per atom.

RESULTS

Composite Structure

Before delving into the discussion of the elastic and fracture properties of these materials, it is useful to briefly describe the intriguing structure that is found to develop in the matrix due to the templating effect of the CNTs. As shown in Figure 2, concentric rings of denser and more highly ordered carbon form at the tube-matrix interface. Closer examination of the structure in these regions reveals a highly defective graphitic structure composed of fused rings with a range of sizes. Below each structural image is the corresponding cylindrical distribution function that shows the deviation from the bulk density as a function of distance from the outermost CNT wall, which is set to r=0 in each graph. In Figure 2a the close spacing between neighboring SWNTs prevents the AC matrix from reaching the bulk density anywhere in the simulation cell. The MWNT array system, shown in Figure 2b, behaves similarly although the greater intertube spacing results in the density fluctuations becoming rather small beyond the tube-tube midpoint distance of 0.8 nm. The SWNT bundle system, shown in Figure 2c, also exhibits small fluctuation features beyond 0.8nm, although the interpretation is complicated by the

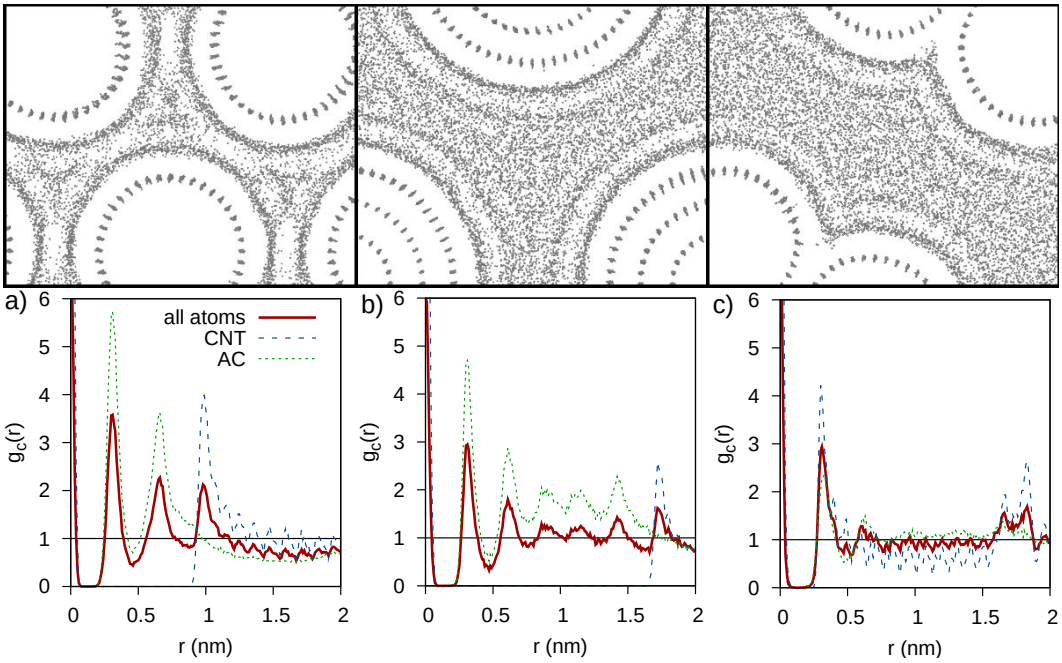

Figure 2. CNT/AC interfaces (top) and cylindrical distribution functions (bottom) for the uncrosslinked (a) SWNT array, (b) MWNT array, and (c) SWNT bundle systems. In the top images, atoms are rendered as 0.02 nm diameter spheres.

presence of overlapping cylindrical shells from neighboring SWNTs. Similar matrix structuring has been previously observed in both experimental and simulation studies [14-15].

Elastic Properties

Figures 3a and 3b plot the dependence of the specific Young's moduli on the degree of crosslinking for deformations in the axial and transverse directions, respectively. For Figure 3b and all following plots showing dependence on crosslinking, the extent of crosslinking is based on the number of CNT carbon atoms directly exposed to the matrix as described above. For 3a, however, an interesting linear decrease was noted for all three systems when the axial specific Young's modulus was plotted versus the absolute degree of crosslinking, which is defined relative to all of the CNT carbons in the system rather than just those exposed to the matrix. All three data sets in Figure 3a show the same decrease of ~4.7 GPa/(g/cm^3) per 1% increase in crosslinking. The fact that this relationship holds for both the SWNT arrays and bundles indicates that the specific axial Young's modulus is independent of the placement of crosslink sites. It is also notable in Figure 3a that the SWNT array system consistently has a larger axial specific modulus than the SWNT array or MWNT systems, which are very close to one another. This could be a result of the additional stiffness provided by induced structure found in the AC matrix in the SWNT array system. Similar CNT-induced structuring has been observed in carbon fiber processing where it was found to promote alignment of the PAN precursor polymer and to increase mechanical properties of the resulting graphitized fiber [16].

Figure 3b shows the relationship between transverse specific Young's modulus and degree of crosslinking. The MWNT array system has the highest transverse specific Young's modulus below 15% crosslinking, after which the SWNT array system becomes comparable. The SWNT bundle system consistently has the lowest transverse specific Young's modulus. The lack of crosslinks between tubes in the bundles means that inter-bundle load transfer is reliant on van der Waals interactions. In the MWNT system, the high transverse stiffness at low crosslinking fractions is likely due to the reinforcing

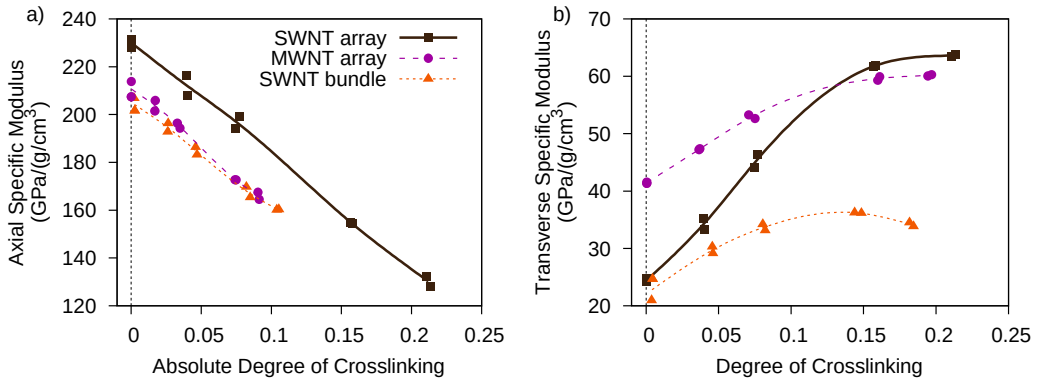

Figure 3. Specific Young's modulus in the (a) axial and (b) transverse directions as a function of crosslinking.

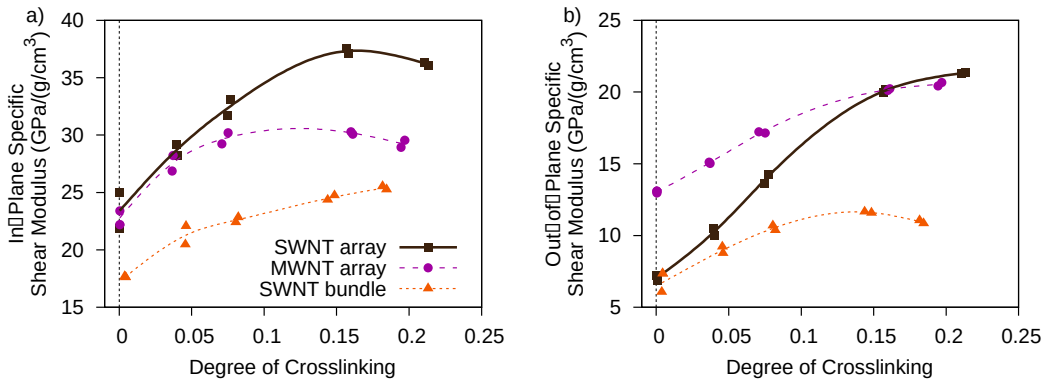

Figure 4. Specific shear modulus in the (a) in-plane and (b) out-of-plane directions, as a function of crosslinking.

effect that the inner walls have in resisting CNT flattening due to the Poisson contraction. The more rapid rise in the SWNT array system simply reflects the larger contact area between the SWNT walls and the AC matrix.

The crosslinking dependences of the in-plane and out-of-plane specific shear moduli are shown in Figures 4a and 4b, respectively. The in-plane component is along the axial direction of the CNTs while the out-of-plane component is in the direction transverse to the CNTs. Increases in the degree of crosslinking results in increases in shear moduli for all systems up to a threshold of ~15%, after which damage to the CNTs caused by crosslink formation begins to deteriorate their ability to sustain shear loads. Also note that the lack of crosslinks between the SWNTs in the SWNT bundles results in significantly reduced moduli in both shear directions.

The calculated Poisson's ratios for each material are shown in Figures 5a and 5b. The major Poisson's ratio corresponds to the transverse response to an applied axial strain while the minor Poisson's ratio corresponds to the response in one transverse direction to a strain applied to the orthogonal transverse direction. The major Poisson's ratios shown in Figure 5a initially increase with increasing crosslinking as more load can be transferred across the interface between the matrix and the CNTs. Above an extent of crosslinking of about 10%, however, increasing integration of the CNTs with the matrix makes the system increasing resistant to transverse compression. As shown in Figure 5b, the minor Poisson's ratios are uniformly larger than the major ratios. This reflects the fact that the circular cross sections of the CNTs are relatively easily deformed when complementary tensile/compressive strains are applied in the two transverse directions. In the case of the major ratio, the uniform compression of the CNT cross-section results in an increased stiffness and corresponding reduction of the Poisson's ratio relative to the minor ratio.

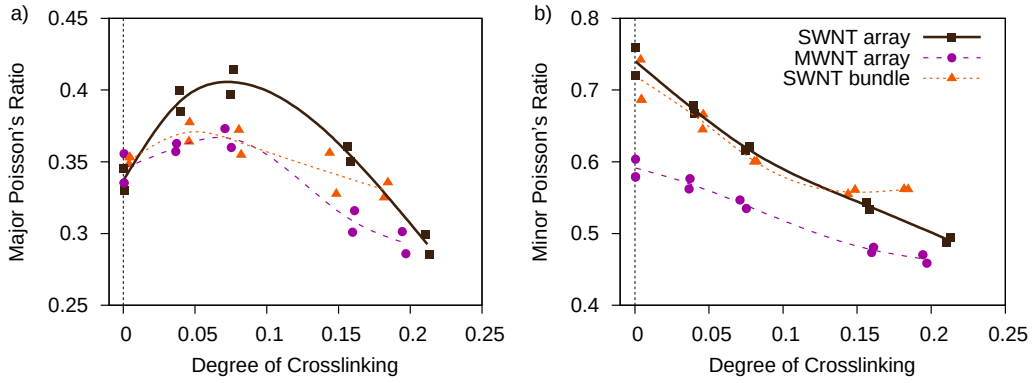

Figure 5. (a) Major and (b) minor Poisson's ratio as a function of crosslinking.

Tensile Fracture Properties

The specific stress-strain responses for deformations in the axial direction are shown for all three CNT systems in Figure 6. The uncrosslinked systems are shown in the left column, while the systems with the highest crosslink fraction considered for each material are shown in the right column. In each plot, the composite specific stress is plotted in green and the specific stresses in the CNTs and the AC matrix are plotted in red and blue, respectively. The two lines plotted for each color correspond to the results obtained for the two independent simulations conducted for each material. There is virtually no difference between the duplicate runs up to strains of about 0.2, indicating that the methods used to generate the starting configurations are robust. Differences at larger strains result from the stochastic nature of the yielding or matrix failure processes, which are uncorrelated with the starting configuration.

Each plot shown in Figure 6 displays a plateau in the specific stress carried by the AC matrix beginning around 0.14 strain, which corresponds to the initiation of fracture in the matrix. As the fracture continues to propagate through the matrix at higher strains, the portion of the specific stress being carried by the CNTs increases. Because the CNTs are carrying nearly all the load after the matrix has failed, the failure strain of the CNTs corresponds very closely with the strain at the point of ultimate strength of the composite. The results shown in Figure 6 also illustrate the significant impact that the crosslinking-induced defects have on the ultimate specific strengths of the CNT composites. As discussed below, optimizing the crosslink fraction is critical in balancing the axial, transverse, and shear performance of these composites.

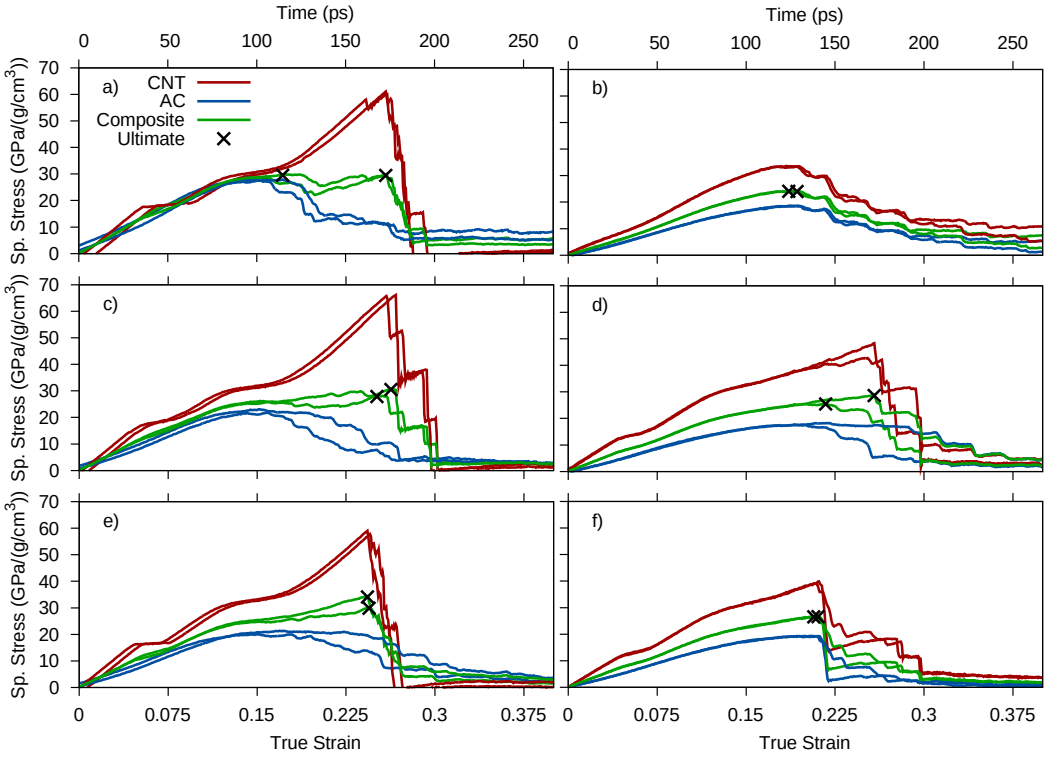

Figure 6. Axial specific stress-strain response of the (a) SWNT array composites 0% crosslinked, (b) SWNT array 21% crosslinked (c) MWNT array composites 0% crosslinked, (d) MWNT array 20% crosslinked (e) SWNT bundle composites 0% crosslinked, (f) SWNT bundle 18% crosslinked.

It is also interesting to look more closely at the systems that feature a mixture of functionalized and unfunctionalized CNTs. For example, in the MWNT system the outermost CNTs are crosslinked to the matrix while the inner CNTs are not. Likewise for the SWNT bundle system, the outer shell of CNTs in each bundle are crosslinked to the matrix while the inner CNT is unfunctionalized. For the array of SWNTs, all of the CNTs were observed to break at essentially the same strain, while the mixture of functionalized and unfunctionalized CNTs found in the MWNT and bundled SWNT systems led to a multistep failure mechanism. Figures 7a and 7b show the specific stress-strain plots for the MWNT system and bundled SWNT systems, respectively, with each tube in the systems plotted individually. The exterior tubes, which are plotted in purple, were crosslinked to the matrix while the interior tubes, shown in orange, were not crosslinked. In both cases, the exterior tubes are seen to fail at much lower strains and to have much lower ultimate strengths than the unfunctionalized inner CNTs. It also notable that there is very little variation in the ultimate specific stress or strain for the functionalized CNTs in either system, indicating that these properties are not strongly dependent on the random variations in the pattern of crosslinks formed to the outer tubes.

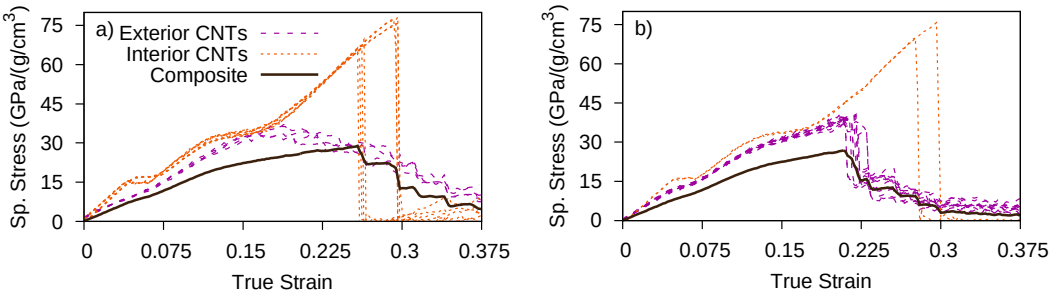

Figure 7. Specific stress-strain response of each individual CNT in the (a) 20% crosslinked MWNT array and (b) 18% crosslinked SWNT bundle.

Using the same layout of systems and crosslinking fractions as Figure 6, Figure 8 displays the specific stress-strain responses for deformations in the transverse direction. It is immediately clear from the left column in Figure 8 that the CNTs bear negligible load in the uncrosslinked systems. In fact, they function as defects in the composite by reducing the strength of the matrix. In the highly crosslinked systems shown in the right column, however, the CNTs are seen to play a significant role in the strength of the composite. The strongest effect is found in the array of SWNTs, because every CNT is

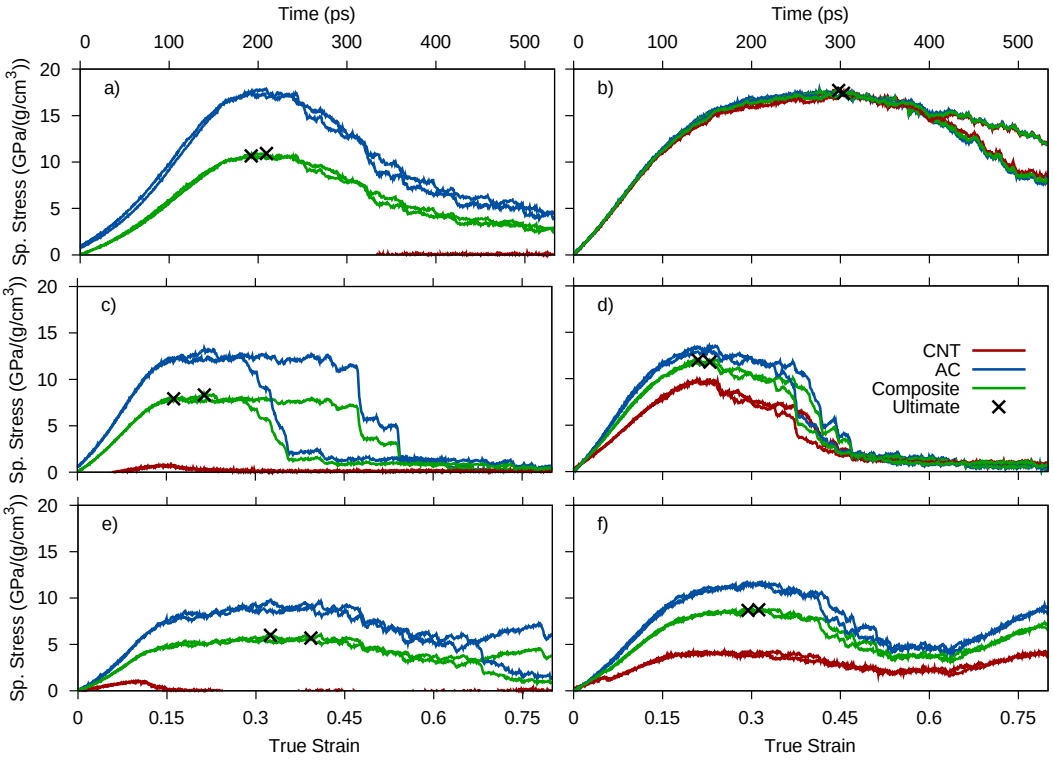

Figure 8. Transverse specific stress-strain response of (a) SWNT array composites 0% crosslinked, (b) SWNT array 21% crosslinked (c) MWNT array composites 0% crosslinked, (d) MWNT array 20% crosslinked (e) SWNT bundle composites 0% crosslinked, (f) SWNT bundle 18% crosslinked.

crosslinked to the matrix. The next most effective reinforcement was the MWNT array system, in which a third of the CNTs contribute to reinforcing the composite. The weakest effect is found for the SWNT bundle system, in which the absence of CNT-CNT crosslinks prevents the bundles from serving as effective transverse reinforcements.

All of the results presented to this point are for the lowest (0%) and highest (~20%) levels of crosslinking. While these data are helpful in understanding the behavior at either extreme, determining optimal degrees of functionalization requires exploration of intermediate cases. Figures 9a and 9b show, respectively, the axial and transverse specific ultimate stresses as a function of the degree of crosslinking for a number of intermediate systems. In the axial direction, it clear that both the SWNT and MWNT array systems reach their maximum strengths at around 4-5% crosslinking. Beyond this point, additional crosslinking only serves to weaken the CNTs and, therefore, the composite. Because of scatter in the data, it is more difficult to identify a clear maximum in the SWNT bundle results, although it appears to fall slightly below 5%, which is consistent with the other systems.

It is interesting that a small degree of crosslinking results in a clear increase in the axial specific ultimate strength while the axial specific Young's modulus was largest for the uncrosslinked system and decreased linearly with crosslinking. Careful inspection of animations of the fracture processes for the uncrosslinked simulations shows that the initial voids nucleate at the CNT-matrix interface. A small degree of crosslinking impedes the formation of these voids, which increases the load required to initiate the fracture process. This reinforcement mechanism is, however, quickly overcome by the damage caused to the CNTs at higher degrees of crosslinking.

The transverse specific ultimate strength results are shown in Figure 9b. While the trend in relative strengths between the three systems is the same as shown in Figure 9a, the behavior with increasing crosslinking is quite different. The MWNT array and SWNT bundle systems appear to plateau or begin decreasing around 20% crosslinking, while the SWNT array system continues to increase at the highest levels considered in this work, reaching a strength increase of 60% over the uncrosslinked system. These results indicate that the weakening of the CNTs caused by increasing degrees of crosslinking is more than compensated for by increased strength in the matrix.

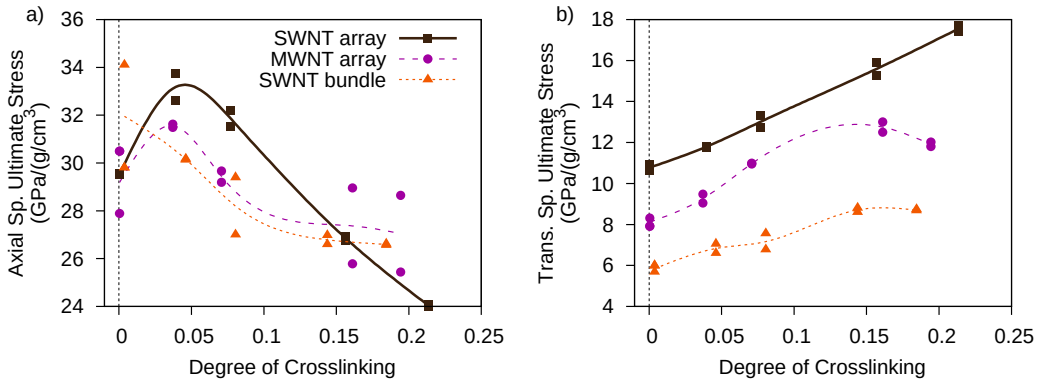

Figure 9. Specific ultimate stress as a function of crosslinking in the (a) axial and (b) transverse directions.

Finally, to place the composite results obtained in the present work in context relative to the constituent materials, Figure 10 plots the axial and transverse specific moduli against the corresponding specific ultimate strengths. The unfilled symbols are results for pure SWNT and MWNT arrays and AC at three densities that are representative of the range found in experimental studies. This previous work was conducted with the same forcefield parameterization used in the present work ($ReaxFF_{C\text{-}2013}$) and used CNTs of the same chirality [4]. Because the specific properties of the pure CNT systems are almost independent of the number of walls in the CNT, the SWNT and MWNT results are nearly indistinguishable in either the axial or transverse directions. This is reflected in the unfilled symbols at the origin and in the extreme upper right corner, representing the transverse and axial CNT properties, respectively. For the pure AC systems, increasing the density results in substantial improvements in specific modulus while the specific strength is weakly dependent on density.

Turning to the composite systems, Figure 10 shows that adding the matrix material results in about a 60% reduction in axial specific ultimate strength and about 45% reduction in axial specific modulus. While the scatter in the points, which results from the various degrees of crosslinking, makes it difficult to draw quantitative conclusions, it does appear that adding the matrix and crosslinks has a slightly more negative effect on axial strength than axial modulus. In the transverse directions, the pure CNT systems have nearly zero modulus and strength. Adding the matrix, even for an uncrosslinked system, results in a composite with reasonably good properties. Adding crosslinks improves both stiffness and strength until they approach the matrix properties.

The predicted knock-downs in axial mechanical properties are expected and echo similar property reductions found in carbon fiber composites. Even after the loss of axial strength and modulus relative to the pure CNTs, these material systems remain very attractive candidates for future composite applications. The near absence of stiffness and strength in the transverse directions prevent the pure CNT systems from being considered for structural applications. The results presented here suggest that with a proper choice of matrix material and judicious crosslinking, their poor transverse properties can be overcome.

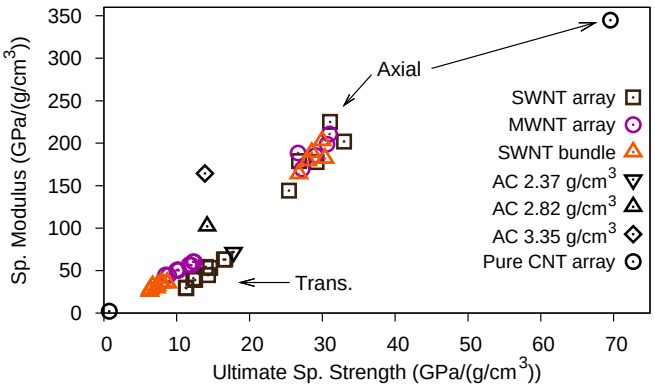

Figure 10. Summary of axial and transverse specific Young's modulus of the composite systems and pure CNT and AC systems from [4] plotted against specific ultimate strength.

CONCLUSIONS

Using molecular dynamics simulations with the ReaxFF potential, specific tensile moduli and specific ultimate strengths were evaluated for a variety of model CNT/AC composite systems. The particular focus was on determining how these mechanical properties depend on the type of CNTs (SWNTs vs MWNTs), how the CNTs were arranged in the simulation (evenly spaced vs bundled), and the extent of crosslinking that existed between the CNTs and the AC matrix (0-20%). While it is not possible to concisely summarize all of the results here, a few notable trends should be mentioned. First, increasing the extent of crosslinking had a uniformly positive effect on transverse specific strengths, specific Young's moduli, and specific shear moduli, due to improved load transfer between the matrix and CNTs. Second, increasing crosslinking has a consistently negative effect on axial specific moduli due to damage to the CNTs that results from crosslink formation. The axial specific strengths, on the other hand, initially increased up to a crosslinking degree of ~5% and then decreased with further crosslinking. Small amounts of crosslinking appear to delay the nucleation of voids at the interface between the CNTs and the AC matrix. Because cracks often initiate at these voids, preventing their formation improves the overall strength of the material. Increasing the extent of crosslinking beyond 5%, however, leads to damage in the CNTs that more than offsets the benefits derived from prevention of void nucleation. Third, the CNTs served as templates for structural ordering in the AC matrix during the equilibration procedure. Several instances were noted in which this induced structure augmented the reinforcing effect of the CNTs. While this effect may be unique to the AC matrix chosen for this work, related work being done with polymeric systems indicates that this phenomenon may be more general [16]. While much remains to be learned, the results presented in this work indicate that it may eventually be possible to fabricate CNT composites with properties exceeding state of the art carbon fiber composites.

ACKNOWLEDGEMENTS

This research was funded by NASA under the Revolutionary Technology Challenges Program (Grant NNX09AM50A). SUPERIOR, a high-performance computing cluster at Michigan Technological University, was used in obtaining some of results presented in this publication.

REFERENCES

1. O'Brien, N. P., M. A. McCarthy. W. A. Curtin. 2013. "Improved inter-tube coupling in cnt bundles through carbon ion irradiation," *Carbon 51* 173-184.
2. Kis, A., G. Csanyi, J. P. Salvetat, T. N. Lee, E. Couteau, A. J. Kulik, W. Benoit, J. Brugger. L. Forro. 2004. "Reinforcement of single-walled carbon nanotube bundles by intertube bridging," *Nat. Mater. 3* (3):153-157.

3. Pukha, V. E., E. N. Zubarev, A. N. Drozdov, A. T. Pugachov, S. H. Jeong. S. C. Nam. 2012. "Growth of nanocomposite films from accelerated C60 ions," *J. Phys. D: Appl. Phys. 45* (33):335302.
4. Jensen, B. D., K. E. Wise. G. M. Odegard. 2015. "Simulation of the elastic and ultimate tensile properties of diamond, graphene, carbon nanotubes, and amorphous carbon using a revised ReaxFF parameterization," *manuscript in preparation*.
5. Plimpton, S. 1995. "Fast parallel algorithms for short-range molecular-dynamics," *J. Comput. Phys. 117* (1):1-19.
6. Aktulga, H. M., J. C. Fogarty, S. A. Pandit. A. Y. Grama. 2012. "Parallel reactive molecular dynamics: Numerical methods and algorithmic techniques," *Parallel Comput. 38* (4-5):245-259.
7. van Duin, A. C. T., S. Dasgupta, F. Lorant. W. A. Goddard, III. 2001. "ReaxFF: A reactive force field for hydrocarbons," *J. Phys. Chem. A 105* (41):9396-9409.
8. Goverapet Srinivasan, S., A. C. T. van Duin. P. Ganesh. 2015. "Development of a ReaxFF potential for carbon condensed phases and its application to the thermal fragmentation of a large fullerene," *J. Phys. Chem. A 119* (4):571-580.
9. Thess, A., R. Lee, P. Nikolaev, H. J. Dai, P. Petit, J. Robert, C. H. Xu, Y. H. Lee, S. G. Kim, A. G. Rinzler, D. T. Colbert, G. E. Scuseria, D. Tomanek, J. E. Fischer. R. E. Smalley. 1996. "Crystalline ropes of metallic carbon nanotubes," *Science 273* (5274):483-487.
10. Alexander, S. 2010. "Visualization and analysis of atomistic simulation data with Ovito–the open visualization tool," *Modell. Simul. Mater. Sci. Eng. 18* (1):015012.
11. Ferrari, A. C., A. Libassi, B. K. Tanner, V. Stolojan, J. Yuan, L. M. Brown, S. E. Rodil, B. Kleinsorge. J. Robertson. 2000. "Density, sp^3 fraction, and cross-sectional structure of amorphous carbon films determined by x-ray reflectivity and electron energy-loss spectroscopy," *Phys. Rev. B 62* (16):11089-11103.
12. Amaratunga, G. A. J., M. Chhowalla, C. J. Kiely, I. Alexandrou, R. Aharonov. R. M. Devenish. 1996. "Hard elastic carbon thin films from linking of carbon nanoparticles," *Nature 383* (6598):321-323.
13. Odegard, G. M., T. S. Gates, L. M. Nicholson. K. E. Wise. 2002. "Equivalent-continuum modeling of nano-structured materials," *Compos. Sci. Technol. 62* (14):1869-1880.
14. Hadden, C. M., B. D. Jensen, A. Bandyopadhyay, G. M. Odegard, A. Koo. R. Liang. 2013. "Molecular modeling of Epon-862/graphite composites: Interfacial characteristics for multiple crosslink densities," *Compos. Sci. Technol. 76* 92-99.
15. Fyta, M. G.. P. C. Kelires. 2005. "Simulations of composite carbon films with nanotube inclusions," *Appl. Phys. Lett. 86* (19):191916.
16. Chae, H. G., Y. H. Choi, M. L. Minus. S. Kumar. 2009. "Carbon nanotube reinforced small diameter polyacrylonitrile based carbon fiber," *Compos. Sci. Technol. 69* (3–4):406-413.